Journal of Nuclear Materials 376 (2008) 247–250

Contents lists available at ScienceDirect

Journal of Nuclear Materials

journal homepage: www.elsevier.com/locate/jnucmat

Letter to the Editor

Ion irradiation damage effects in δ-phase $Y_6W_1O_{12}$

M. Tang *, J.A. Valdez, K.E. Sickafus

Materials Science and Technology Division, Mail-Stop G755, Los Alamos National Laboratory, Los Alamos, NM 87545, USA

ARTICLE INFO

Article history:
Received 4 February 2008
Accepted 9 March 2008

PACS:
81.05.Je
61.80.Jh
61.16.Bg
61.05.Cp
61.50.Ks

ABSTRACT

Polycrystalline $Y_6W_1O_{12}$ samples were irradiated with 280 keV Kr^{2+} ions to fluences up to 2×10^{20} ions/m^2 at cryogenic temperature (100 K). Ion irradiation damage effects in these samples were examined using grazing incidence X-ray diffraction (GIXRD) and cross-sectional transmission electron microscopy (TEM). The pristine $Y_6W_1O_{12}$ possesses rhombohedral symmetry (structure known as the δ-phase), which is closely related to cubic fluorite structure. GIXRD and TEM observations revealed that the irradiated $Y_6W_1O_{12}$ experiences an ordered rhombohedral to disordered cubic fluorite transformation by a displacement damage dose of ~12 displacements per atom (dpa). At the highest experimental dose of ~50 dpa, the uppermost irradiated region was found to be partially amorphous while the buried damage region was found to contain the same fluorite structure as observed at lower dose.

A number of studies have been published in recent years regarding the radiation damage behavior of fluorite derivative compounds, i.e., compounds with crystal structures closely related to the fluorite (CaF_2) crystal structure. Most notably, these studies include $A_2B_2O_7$ pyrochlore (see, e.g., [1–3]) and $A_4B_3O_{12}$ delta (δ)-phase compounds [4–6]. The purpose of this letter is to report preliminary results on radiation damage effects in a related fluorite derivative compound, $Y_6W_1O_{12}$. $Y_6W_1O_{12}$ is a compound with $A_6B_1O_{12}$ stoichiometry that crystallizes with a structure analogous to the $A_4B_3O_{12}$ δ-phase compounds. Both $A_6B_1O_{12}$ (6:1:12) and $A_4B_3O_{12}$ (4:3:12) δ-phase compounds can be described as M_7O_{12} compounds with rhombohedral distortions compared to the ideal, cubic MO_2 fluorite structure. Also, these compounds possess ordered arrangements of oxygen 'vacancies' that accommodate the oxygen deficiency of M_7O_{12} ($MO_{1.714}$) compounds compared to MO_2. The main differences between 4:3:12 and 6:1:12 δ-phase compounds are the cations used to produce the respective stoichiometries: 4:3:12 compounds are made from trivalent and tetravalent cations ($A_4^{3+}B_3^{4+}O_{12}$), while 6:1:12 compounds incorporate trivalent and hexavalent species ($A_6^{3+}B_1^{6+}O_{12}$). Compounds with 6:1:12 stoichiometry utilize cation mixtures such as A = Y, RE (RE = rare earth element) and B = W, Mo, Re, U (e.g., $Yb_6W_1O_{12}$, $Y_6U_1O_{12}$).

The crystal structure of the compound we report on here (shown in Fig. 1), δ-$Y_6W_1O_{12}$, belongs to space group $R\bar{3}$ [7,8] and possesses a superstructure compared to the parent fluorite phase, due to ordering of both the Y and W cations on the cation sublattice, as well as the oxygen 'vacancies' on the anion sublattice [7]. The W^{6+} cations occupy the 3*a* Wyckoff equipoint in VI-fold, distorted octahedral coordination relative to nearest-neighbor oxygen anions, while the Y^{3+} cations occupy the general 18*f* equipoint with VII-fold coordination relative to surrounding O anions. The formally vacant anion sites, relative to the ideal MO_2 parent fluorite phase, are located at the 6*c* equipoint positions on the triad axes. There is also some relaxation of the O anions from their ideal fluorite positions around these vacant sites.

This article describes structural changes induced in δ-$Y_6W_1O_{12}$ by heavy ion irradiation at cryogenic temperature. The ions used in this study were 280 keV Kr^{2+} ions and the temperature of the samples prior to irradiation was ~100 K. The displacement damage dose range investigated here was ~12–50 displacements per atom (dpa).

High purity WO_3 and Y_2O_3 powders from Alfa Aesar (99.998% and 99.99% pure) were used in the molar ratio of 1:3 to produce sintered oxide pellets of composition $Y_6W_1O_{12}$. X-ray diffraction measurements showed that the sintered pellets possess the so-called 'δ-phase' crystal structure, a structure characterized by rhombohedral symmetry. Ion irradiations were performed at cryogenic temperature (~100 K) in the Ion Beam Materials Laboratory at Los Alamos National Laboratory, using a Varian ion implanter operating at 140 kV. 280 keV Kr^{2+} ions were implanted at normal incidence using a dose rate of 3.2×10^{16} Kr/m^2 s to fluences ranging from 0.5 to 2×10^{20} Kr/m^2. Irradiated samples were analyzed using both grazing incidence X-ray diffraction (GIXRD) and transmission electron microscopy (TEM). GIXRD measurements were

* Corresponding author. Tel.: +1 505 665 1472; fax: +1 505 667 8021.
E-mail address: mtang@lanl.gov (M. Tang).

0022-3115/$ - see front matter © 2008 Elsevier B.V. All rights reserved.
doi:10.1016/j.jnucmat.2008.03.008

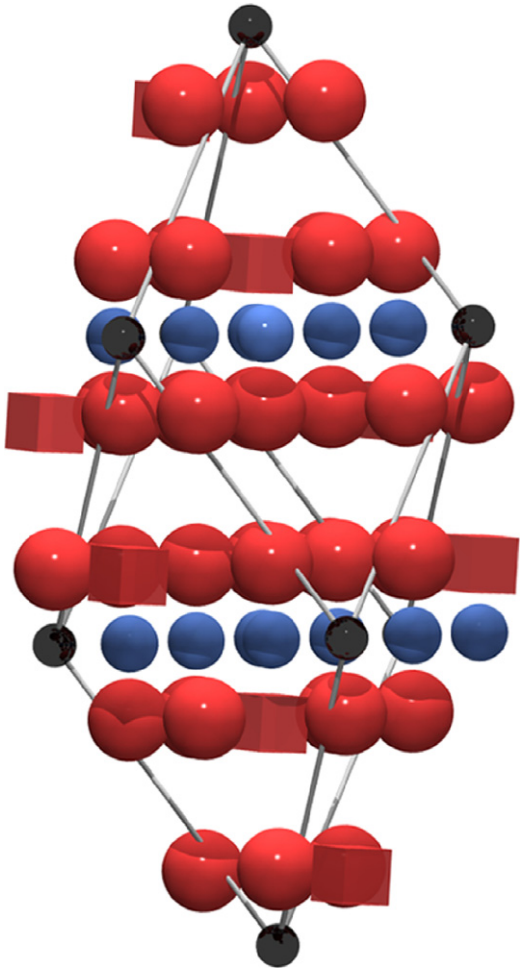

Fig. 1. Schematic diagram showing the *idealized* (unrelaxed) rhombohedral unit cell of δ-$Y_6W_1O_{12}$. The cell contains one molecule ($Z = 1$), with 1 W cation at the origin (black), and 6 Y cations (blue) and 12 oxygen anions (red) in the cell interior. Extra atoms outside the unit cell are shown in this drawing to emphasize the atom layers perpendicular to the rhombohedral cell axis. The layers consist of pure cations (W/Y) and pure anions (O), with two adjacent O layers per W/Y layer. The red cubes represent 'missing' O anions, compared to the ideal, fluorite (CaF_2) crystal structure. The rhombohedral unit cell is exaggerated along the axis of the rhombohedral unit cell to emphasize the 'layered' structure along this axis. (For interpretation of the references in color in this figure legend, the reader is referred to the web version of this article.)

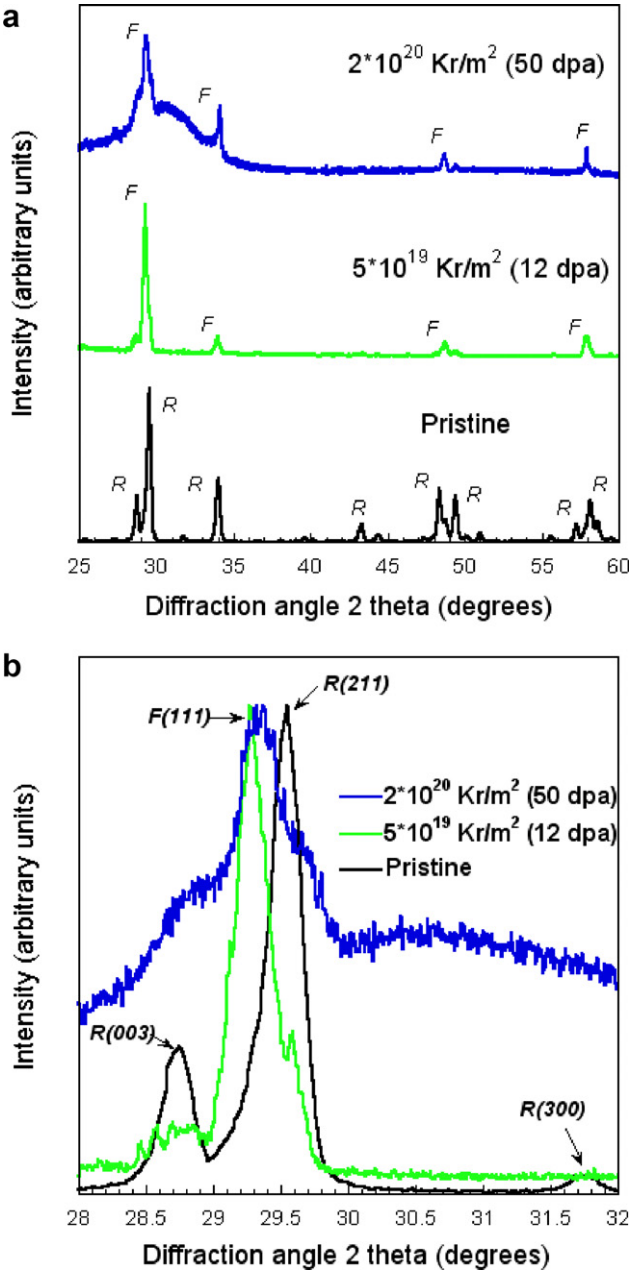

Fig. 2. (a) Grazing incidence X-ray diffraction (GIXRD) patterns obtained from $Y_6W_1O_{12}$ before and after irradiation with 280 keV Kr^{2+} ions. (b) Expanded view of GIXRD patterns in (a) over the range $2\theta = 28–32°$.

performed using a Bruker AXS D8 Advanced X-ray diffractometer. Irradiated samples were prepared in cross-sectional geometry for TEM examination. TEM investigations were performed using Philips CM-30 and FEI Tecnai F30 electron microscopes operating at 300 kV.

Fig. 2(a) shows GIXRD patterns obtained from pristine $Y_6W_1O_{12}$ and $Y_6W_1O_{12}$ irradiated with 280 keV Kr^{2+} ions to fluences of 5×10^{19} Kr/m^2 and 2×10^{20} Kr/m^2. These ion fluences correspond to peak displacement damage doses of ~12 and 50 dpa (these are estimates based on the Monte Carlo ion transport code SRIM [9]; 40 eV was used for the displacement threshold energy for all target atoms in these calculations). The pristine GIXRD pattern in Fig. 2(a) is consistent with the rhombohedral δ-phase $Y_6W_1O_{12}$ structure (diffraction peaks labeled 'R'). Upon ion irradiation to a fluence of 5×10^{19} Kr/m^2, most of the pristine R peaks disappear, leaving four prominent diffraction peaks in the range $2\theta = 25–60°$ (labeled 'F' in Fig. 2(a)). These peaks can be interpreted as arising from a phase with a fluorite structure. In this case, these four peaks index as {111}, {200}, {220}, and {311}, with increasing scattering angle. When the irradiation fluence is increased to 2×10^{20} Kr/m^2, a broad diffraction feature emerges in the scattering angle $2\theta = 25–60°$ (Fig. 2(a)). This diffraction is interpreted as arising from an amorphous structure formed at this irradiation dose of 50 dpa. Fig. 2(b) shows the same GIXRD patterns as in Fig. 2(a), in the low-angle range $28° < 2\theta < 32°$. The rhombohedral peaks R(003), R(211), and R(300) are strongly diminished with increasing radiation dose. Simultaneously, a peak labeled F(111) emerges by an ion dose of 12 dpa, which is interpreted as arising from an irradiation-induced fluorite structure. Finally, a broad diffraction feature due to an amorphous structure is observed at the high experimental dose of 50 dpa.

Fig. 3 shows a cross-sectional TEM image obtained from $Y_6W_1O_{12}$ irradiated with 280 keV Kr^{2+} ions to a fluence of 5×10^{19} Kr/m^2 (corresponding to ~12 dpa). The inset microdiffrac-

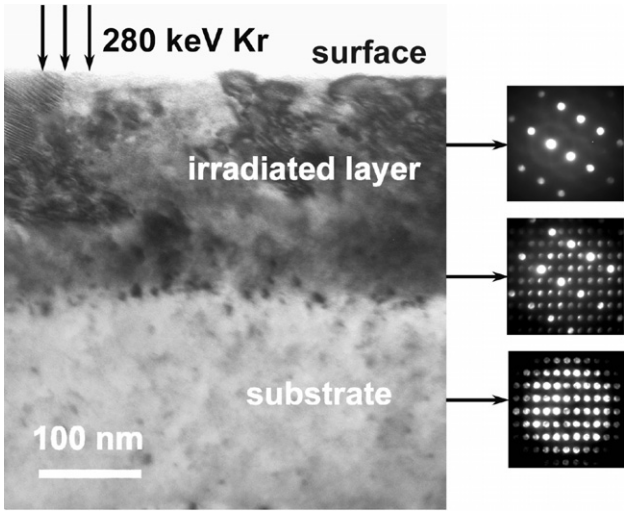

Fig. 3. Cross-sectional TEM bright-field image (left) and microdiffraction (μD) patterns (right) for $Y_6W_1O_{12}$ irradiated to a fluence of 5×10^{19} Kr/m^2 (~12 dpa). The disappearance of specific diffraction spots (top μD pattern) suggests that there is O–D phase transformation in the irradiated $Y_6W_1O_{12}$. The middle μD pattern was obtained near the interface between the irradiated and unirradiated materials, and thus contains contributions from structures in both regions.

tion (μD) patterns indicate a change in structure between the unirradiated substrate (bottom pattern) and the irradiated layer (top pattern). The middle μD pattern was obtained near the interface between the substrate and the bottom of the irradiated layer and thus may contain contributions from both structures. The substrate μD pattern is consistent with the rhombohedral δ-phase $Y_6W_1O_{12}$ structure. Superlattice reflections characteristic of pristine $Y_6W_1O_{12}$ are seen to disappear in the μD pattern obtained from the irradiated layer. This μD pattern from the irradiated layer can be indexed as consistent with a cubic, disordered fluorite phase. The middle μD pattern in Fig. 3 clearly shows the superlattice reflections associated with the rhombohedral δ-phase, as well as the brighter, fundamental fluorite reflections.

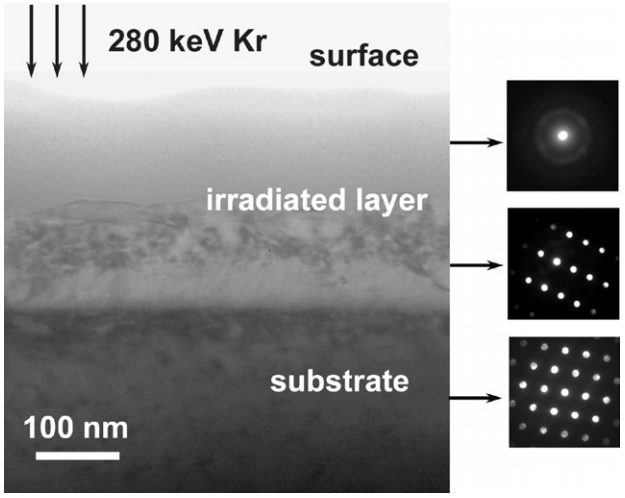

Fig. 4. Cross-sectional TEM bright-field image (left) and microdiffraction (μD) patterns (right) for $Y_6W_1O_{12}$ irradiated to a fluence of 2×10^{20} Kr/m^2 (~50 dpa). The diffuse halo in top μD pattern indicates a partial amorphization transformation has occurred in the surface layer of irradiated $Y_6W_1O_{12}$. The μD pattern obtained from the middle layer below the amorphous top layer, reveals that a disordered fluorite layer was formed in this region.

Fig. 4 shows a cross-sectional TEM image obtained from $Y_6W_1O_{12}$ irradiated with 280 keV Kr^{2+} ions to a fluence of 2×10^{20} Kr/m^2 (corresponding to ~50 dpa). Three regions with different diffraction contrast are apparent from top to bottom in the image. The bottom area is the unirradiated substrate, while the top and middle layers comprise the Kr^{2+} ion irradiated damage region. The diffuse halo in μD pattern corresponding to the top layer indicates that this high-dose irradiated $Y_6W_1O_{12}$ possesses a partially amorphized surface layer (thickness ~100 nm). Below the amorphous top layer, the corresponding μD pattern in middle layer is consistent with a fluorite structure (thickness ~80 nm), equivalent to the structure in the irradiated region in Fig. 3. The structural changes observed in the high-dose ion irradiated δ-phase $Y_6W_1O_{12}$ sample were further investigated using high-resolution TEM (HRTEM). Fig. 5 shows HRTEM micrographs obtained from the same sample as in Fig. 4 at the following positions: (a) the topmost surface of the irradiated region, and (b) the interface between lower irradiated layer and unirradiated substrate. These micrographs were obtained with the electron beam aligned along $\vec{B} = [1\,2\,1]$ with respect to the rhombohedral δ-phase $Y_6W_1O_{12}$ substrate

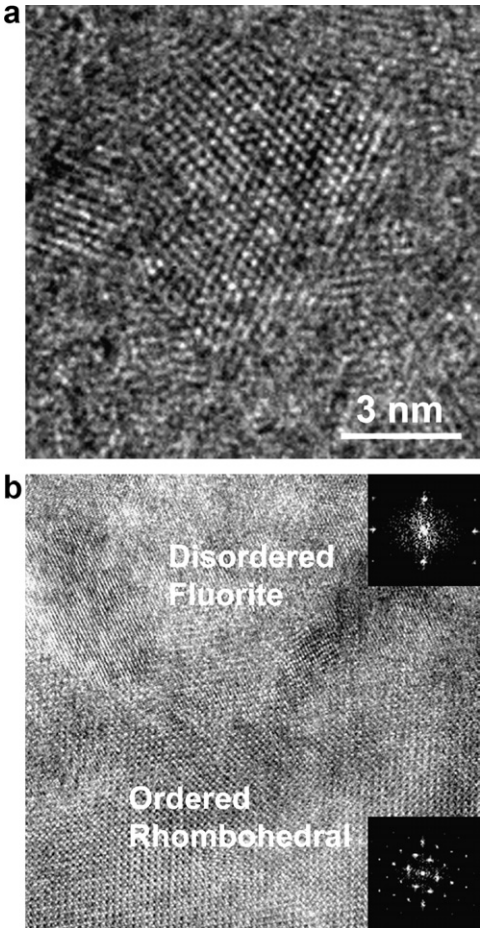

Fig. 5. High-resolution TEM (HRTEM) micrographs obtained from regions of the same irradiated sample as in Fig. 4: (a) the topmost surface region of the irradiated sample; (b) the interface between the lower irradiated region and the unirradiated substrate. The micrograph in (a) reveals the presence of nano-sized crystalline domains embedded in an amorphous matrix. The micrograph in (b) was obtained with the electron beam aligned along the [1 2 1] direction with respect to the rhombohedral δ-phase $Y_6W_1O_{12}$ substrate (using the 3-index system for indexing hexagonal directions). The beam direction for irradiated layer is consistent with a cubic fluorite structure with viewed along $[\bar{1}\,1\,2]$. Diffractograms in (b) were obtained by fast Fourier transforms (FFT) from HRTEM image regions labeled 'ordered rhombohedral' and 'disordered fluorite'. These FFTs are consistent with the μD patterns shown in Fig. 4.

(using the 3-index system for indexing hexagonal directions). Fig. 5(a) revealed that the upper damage region consists of nano-sized crystalline domains embedded in an amorphous matrix. In Fig. 5(b), two distinct structural regions, labeled 'ordered rhombohedral' and 'disordered fluorite', are apparent. Insets shown in Fig. 5(b) are diffractograms obtained using the fast Fourier transform (FFT) method, from the ordered and disordered regions in the HRTEM micrograph. These diffractograms are consistent with the μD patterns in Fig. 4. The HRTEM observations confirm that Kr^{2+} ion irradiation induces a partially amorphous layer in the uppermost irradiated layer of $Y_6W_1O_{12}$, and a fluorite-structural region in the buried irradiated layer.

GIXRD and TEM observations indicate an irradiation-induced phase transformation sequence in $Y_6W_1O_{12}$, progressing from an ordered, δ-phase structure with rhombohedral symmetry to a fluorite phase with cubic symmetry by a dose of ~12 dpa, and finally to a partially amorphous phase by the highest experimental dose of ~50 dpa. The first transformation to the cubic fluorite phase is interpreted as an order-to-disorder (O–D) transformation, analogous to that seen in previous radiation damage studies on 4:3:12 δ-phase compounds, particularly δ-$Sc_4Zr_3O_{12}$ [4] and in addition, δ-$Lu_4Zr_3O_{12}$ [5]. It is interesting that in pristine δ-$Y_6W_1O_{12}$, both the cation and anion sublattices are reportedly highly ordered [7]. In such a compound, the O–D transformation necessarily involves disordering of both the cation and anion sublattices [5]. In the 4:3:12 δ-phase compounds, the cation sublattices are typically disordered in the as-synthesized state (or in some instances, weakly ordered) [7]. In these compounds, disordering on the anion sublattice is sufficient to induce an O–D transformation. In δ-$Y_6W_1O_{12}$, on the other hand, the radiation-induced O–D transformation involves cation antisite reactions ($A_A + B_B \rightarrow A_B + B_A$, where A_A represents an A cation on an A site, A_B represents an A cation on a B site; similar definitions apply for B_B and B_A) and anion Frenkel reactions ($O_O \rightarrow V_O + O_i$, where O_O represents an O anion on an O site, V_O represents an O vacancy, and O_i represents an O interstitial) [5]. In the process of these reactions, the rhombohedral symmetry of the ordered δ-phase vanishes in favor of cubic symmetry, and the material transforms to a structure indistinguishable from the fluorite (CaF_2) crystal structure. We refer to this radiation-induced structure as a 'disordered fluorite' phase. The defect reactions described above that lead to this O–D transformation of δ-phase compounds are analogous to those in $A_2B_2O_7$ pyrochlore compounds [3]. Pyrochlore compounds also undergo O–D transformations from an ordered fluorite derivative structure to a disordered fluorite phase under irradiation (see, e.g., [2]).

The irradiation-induced amorphization transformation observed in this study at high-dose (~50 dpa) has not been reported before for radiation damage studies of δ-phase compounds. One factor that may contribute to the amorphization transformation observed here is the large disparity between the ionic radii of the W^{6+} and Y^{3+} cations. This large size difference is not favorable to cation antisite reactions, thus limiting the atomic mechanisms available for lattice recovery from radiation damage [10]. Assuming that all of the W^{6+} cations reside on the 3*a* Wyckoff position in the $R\bar{3}$ unit cell and are VI-fold coordinated to nearest-neighbor O anions, and all of the Y^{3+} cations reside on the 18*f* equipoint and are VII-fold coordinated by O anions [7], then the W/Y cation radius ratio is given by $r(Y^{3+}_{VII})/r(W^{6+}_{VI}) = 0.96/0.6 = 1.6$ (based on Shannon ionic radii [11]). This ratio should be compared with those corresponding to δ-$Sc_4Zr_3O_{12}$ and δ-$Lu_4Zr_3O_{12}$, wherein no amorphization transformations were observed in radiation experiments to similar or higher doses compared to this study [4,5]. Assuming that the cation sublattices in these δ-phase compounds are randomized, their cation radius ratios are given by

$$\left\langle r\left(Sc^{3+}_{VI,VII}\right)\right\rangle \Big/ \left\langle r\left(Zr^{4+}_{VI,VII}\right)\right\rangle = 0.80/0.77 = 1.04 \quad (1)$$

and

$$\left\langle r\left(Lu^{3+}_{VI,VII}\right)\right\rangle \Big/ \left\langle r\left(Zr^{4+}_{VI,VII}\right)\right\rangle = 0.91/0.77 = 1.18\ [11] \quad (2)$$

Clearly, the cation radius ratio in our 6:1:12 compound is much larger than in the 4:3:12 compounds studied previously. Work is in progress on additional 6:1:12 compounds to determine if the cation radius ratio is indeed an important parameter in determining susceptibility to radiation-induced amorphization.

In summary, Kr ion irradiation experiments under cryogenic conditions on polycrystalline δ-phase $Y_6W_1O_{12}$ was performed. GIXRD measurements and TEM observations revealed two irradiation-induced phase transformations: first, an order-to-disorder (O–D) transformation from the ordered rhombohedral δ-phase structure to disordered fluorite structure at a displacement damage dose of 12 dpa; second from the disordered fluorite structure to partially amorphous at a displacement damage dose of 50 dpa. We propose that the initial phase transformation to a fluorite structure involves cation antisite reactions and anion Frenkel pair defects.

Acknowledgements

This work was sponsored by the Seaborg Institute for Transactinium Science, Los Alamos National Laboratory (LANL), and the US Department of Energy (DOE), Office of Basic Energy Sciences (OBES), Division of Materials Sciences and Engineering.

References

[1] J. Lian, J. Chen, L.M. Wang, R.C. Ewing, J. Matt Farmer, L.A. Boatner, K.B. Helean, Phys. Rev. B 68 (2003) 134107.
[2] R.C. Ewing, W.J. Weber, J. Lian, J. Appl. Phys. 95 (2004) 5949.
[3] K.E. Sickafus, L. Minervini, R.W. Grimes, J.A. Valdez, M. Ishimaru, F. Li, K.J. McClellan, T. Hartmann, Science 289 (2000) 748.
[4] J.A. Valdez, M. Tang, K.E. Sickafus, Nucl. Instrum. and Meth. B 250 (2006) 148.
[5] K.E. Sickafus, R.W. Grimes, J.A. Valdez, A. Cleave, M. Tang, M. Ishimaru, S.M. Corish, C.R. Stanek, B.P. Uberuaga, Nat. Mater. 6 (2007) 217.
[6] M. Ishimaru, Y. Hirotsu, M. Tang, J.A. Valdez, K.E. Sickafus, J. Appl. Phys. 102 (2007) 063532.
[7] H.J. Rossell, H.G. Scott, J. Phys. (Paris) Colloq. 38 (1977) C7.
[8] K. Kuribayashi, M. Yoshimura, T. Ohta, T. Sata, J. Am. Ceram. Soc. 63 (1980) 644.
[9] J.F. Ziegler, J.P. Biersack, U. Littmark, The Stopping and Range of Ions in Solids, Pergamon, New York, 1985.
[10] K.E. Sickafus, A.C. Larson, N. Yu, M. Nastasi, G.W. Hollenberg, F.A. Garner, R.C. Bradt, J. Nucl. Mater. 219 (1995) 128.
[11] R.D. Shannon, Acta Crystallogr. A 32 (1976) 751.